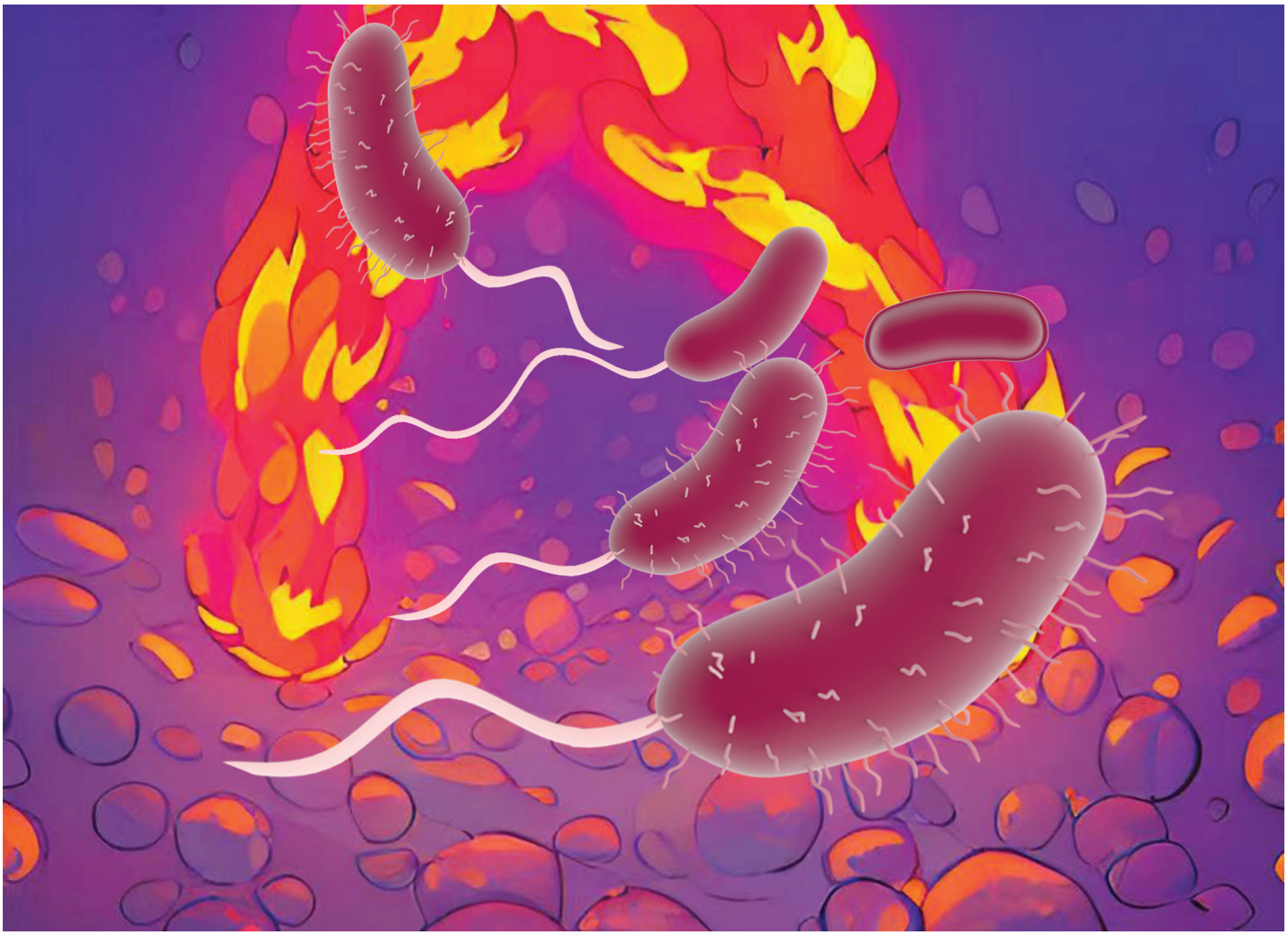

**Showcasing research from Prof. Yuanyuan Wang's group at School and Hospital of Stomatology, Peking University and Prof. Zhiqiang Lin's group at School of Basic Medical Sciences, Peking University, Beijing, China.**

Engineering core–shell chromium nanozymes with inflammation-suppressing, ROS-scavenging and antibacterial properties for pulpitis treatment

Chromium nanozymes (NanoCr), selected from dozens of metallic nanoparticles with core–shell structures, have demonstrated excellent biocompatibility and multienzyme activity. NanoCr has shown effective inhibition against various common pathogens causing oral infections and has the ability to suppress inflammation reactions. This balance between biocompatibility, anti-inflammatory capacity, and antibacterial performance makes NanoCr a promising therapeutic strategy for clinical pulpitis.

## As featured in:

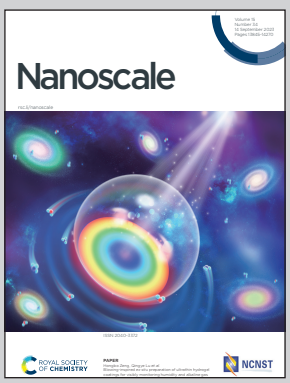


See Zhiqiang Lin, Yuanyuan Wang *et al.*, *Nanoscale*, 2023, **15**, 13971.

ROYAL SOCIETY OF CHEMISTRY

rsc.li/nanoscale

Registered charity number: 207890

Nanoscale

PAPER



Cite this: *Nanoscale*, 2023, **15**, 13971

# Engineering core–shell chromium nanozymes with inflammation-suppressing, ROS-scavenging and antibacterial properties for pulpitis treatment†

Fei Xie, ‡[a] Chuanda Zhu, ‡[b,c] Lidong Gong, [b] Ningxin Zhu,[a] Qiang Ma, [d] Yuanyuan Yang,[b] Xinrong Zhao, [e] Man Qin,[a] Zhiqiang Lin *[b] and Yuanyuan Wang *[a]

Oral diseases are usually caused by inflammation and bacterial infection. Reactive oxygen species (ROS), which come from both autologous inflammation tissue and bacterial infection, play an important role in this process. Thus, the elimination of excessive intracellular ROS can be a promising strategy for anti-inflammatory treatment. With the rapid development of nanomedicines, nanozymes, which can maintain the intracellular redox balance and protect cells against oxidative damage, have shown great application prospects in the treatment of inflammation-related diseases. However, their performance in pulpitis and their related mechanisms have yet to be explored. Herein, we prepared dozens of metallic nanoparticles with core–shell structures, and among them, chromium nanoparticles (NanoCr) were selected for their great therapeutic potential for pulpitis disease. NanoCr showed a broad antibacterial spectrum and strong anti-inflammatory function. Antibacterial assays showed that NanoCr could effectively inhibit a variety of common pathogens of oral infection. *In vitro* experiments offered evidence of the multienzyme activity of NanoCr and its function in suppressing ROS-induced inflammation reactions. The experimental results show that NanoCr has optimal antibacterial and anti-inflammatory properties in *in vitro* cell models, showing great potential for the treatment of pulpitis. Therefore, the use of NanoCr could become a new therapeutic strategy for clinical pulpitis.

Received 19th June 2023,
Accepted 10th August 2023

DOI: 10.1039/d3nr02930a

rsc.li/nanoscale

## 1. Introduction

As one of the most common oral diseases, pulpitis has received close attention. Pulpitis is a disease related to infection and inflammation and is also closely related to sepsis, cardiovascular and cerebrovascular diseases and other noninfectious diseases.[1,2] Normal dental pulp tissue is composed mainly of various cells and extracellular matrix and has many physiological functions, such as vascular differentiation, innervation, immune ability and nerve sensation.[3,4] In general, numerous opportunistic pathogens, such as *Escherichia coli* and *Enterococcus faecalis*, remain latent in the oral environment for extended periods.[5] When mechanical injury occurs in the body, opportunistic pathogens colonize the injured part of the oral cavity and further produce proinflammatory substances (such as endotoxin) to induce an inflammatory response in dental pulp cells. In fact, inflammation has two functions in the treatment of dental pulp. Mild inflammation in the oral cavity can be used as a protective reaction to promote the immune efficacy of dental pulp cells against invading organisms and repair tissue damage. However, a strong inflammatory immune response leads to severe irreversible damage to the dental pulp nerve and can even eventually lead to the loss of dental organs.[6]

The main methods to treat pulpitis are indirect pulp treatment, pulpotomy and root canal treatment. The former two methods, also known as vital pulp therapy, aim to save as much vital pulp as possible to improve the long-term survival of teeth, especially for immature permanent teeth with root dysplasia and thin dentin walls.[3,7,8] The success of vital pulp therapy is related to many factors, such as the determination of pulp status, the developmental stage of teeth, the degree of contamination, and the choice of lining or capping

[a]*Department of Pediatric Dentistry, School and Hospital of Stomatology, Peking University, Beijing 100081, P.R. China. E-mail: cwyyd@126.com*
[b]*Institute of Systems Biomedicine, School of Basic Medical Sciences, Beijing Key Laboratory of Tumor Systems Biology, Peking University Health Science Center, Beijing 100191, P.R. China. E-mail: zhiqiang_lin@bjmu.edu.cn*
[c]*Department of Biochemistry and Biophysics, School of Basic Medical Sciences, Peking University Health Science Center, Beijing 100191, P.R. China*
[d]*Institute of Environment and Sustainable Development in Agriculture, Chinese academy of Agriculture, Beijing 100081, P.R. China*
[e]*Center of Medical and Health Analysis, Peking University Health Science Center, Beijing 100191, P.R. China*
†Electronic supplementary information (ESI) available. See DOI: **https://doi.org/10.1039/d3nr02930a**
‡These authors contributed equally to this work and should be considered co-first authors.

materials.[9–11] Among these factors, the choice of lining or pulp capping materials is of great importance to the success of vital pulp therapy. Pulp capping materials are designed to protect exposed dentin and pulp from external stimuli by placing biomaterials over the pulp, thereby eliminating contact with microbial stimuli and preventing new bacterial damage. Regarding treatment, pulp capping is faster, simpler and less invasive than pulpotomy and root canal therapy. In brief, the ideal pulp capping material for pulpitis should have the following advantages: favorable antibacterial performance, strong anti-inflammatory capacity and a capacity for long-term maintenance of pulp vitality.[12–14]

Currently, numerous organic and inorganic materials, including calcium hydroxide (CH) and calcium silicate materials, are used to prepare pulp capping materials to prevent infection and reduce inflammatory reactions. CH has also received much attention since its development and is considered the gold standard pulp capping material in research. However, CH is limited by its poor sealing performance, its unsatisfactory anti-inflammatory effect and necrosis of the pulp surface after pulp capping.[15,16] While calcium silicate materials, such as mineral trioxide aggregate (MTA), have the advantages of better sealing and better biocompatibility than CH, the problem of strong inflammatory reactions in dental pulp tissue still hinders their further promotion and application.[17–19] In addition, the antibacterial and antifungal properties of MTA remain controversial, and its antibacterial effect on common infectious microorganisms is limited. For example, MTA has no antibacterial activity against anaerobic bacteria.[20,21] The traditional pulp capping materials mentioned above are still widely flawed in practical applications due to suboptimal performance in all but one treatment factor, so there is an urgent need to explore new safe and effective strategies for the treatment of pulpitis.

Reactive oxygen species (ROS) are important signaling molecules in normal cells. Different antioxidant active enzymes, such as superoxide dismutase (SOD), glutathione peroxidase (GSH-Px) and catalase (CAT), can keep ROS in a balanced state, limiting their damage to cells.[22–24] However, excessive ROS accumulation in inflammatory tissues can not only upregulate inflammatory reactions but also inhibit the function of endogenous stem cells to obstruct tissue repair and regeneration.[25] Apart from ROS generated from autologous inflammation tissue, ROS from bacterial infection can also induce significant damage, resulting in both acute and chronic inflammation.[26,27] Therefore, the elimination of excessive intracellular ROS can be a promising strategy for anti-inflammatory treatment. Nanozymes have been recently acknowledged as a promising medicine to maintain the intracellular redox balance and protect cells against oxidative damage. These enzyme-mimetic nanomaterials, including metal/metal oxide-doped carbon-based artificial nanozymes (Pt, Pd, Fe, Co, Cu, Ni, and Ce), have many advantages compared with natural enzymes, such as stability, reproducibility, higher design flexibility, low cost and multienzyme activity.[22,28] Studies have shown that a series of nanomaterials, including $Mn_3O_4$, $CeO_2$, $MnO_2$ and Pt nanoparticles, exhibit excellent biomimetic activity to relieve oxidative conditions.[25,29–31] Furthermore, nanozymes perform as catalases and are able to convert endogenous $H_2O_2$ into $O_2$. Hence, CAT mimetic nanozymes can not only assuage hypoxia in local tissue but also improve anaerobic conditions, which are critical for anaerobic bacteria.[25] In summary, nanozymes can be a promising solution to dental pulpitis, which is closely related to both inflammation and infection.

However, challenges in the use of metallic nanozymes to treat infection and inflammation remain to be solved before they can be implemented for clinical pulpitis treatment. First, pulp is in the deep tissue of hard dentin. Especially when a bacterial biofilm is formed, the diffusion depth of metal ions is greatly limited due to the existence of its extracellular polymer. Second, the pathogenesis of pulpitis is essentially attributed to the overactive immune response caused by the exposure of dental pulp tissue to microorganisms. In this process, inflammatory bodies play a central role in microbial and damage perception, as well as signal transduction and regulation of innate immunity. To some extent, the progression of inflammation can be effectively alleviated by inhibiting relevant immune pathways. Third, dental pulp cells are relatively fragile and can hardly survive the toxicity of most metal ions. Research on the treatment of pulpitis focuses mainly on reducing inflammatory reactions and sterilization while ignoring the possibility of pulp cell death. Therefore, in the treatment of pulpitis, a conflict remains between the biocompatibility, anti-inflammatory capacity and antibacterial performance of pulp capping materials. It is important to achieve a balance between the above treatment factors to obtain a favorable treatment effect.

As a result of the abovementioned challenges, we constructed lipid nanoparticles based on metal ions by the reverse microemulsion threshold precipitation method. In this work, metal ion nanoparticles with superior biocompatibility were selected to test both their antibacterial and inflammatory regulatory abilities. Among the selected nanoparticles were those with chromium phosphate cores and polyethylene glycol phospholipid bilayers, which form a spherical core–shell structure used as a metal ion carrier. In brief, we first prepared dozens of metallic nanoparticles and then performed further screening to identify those with excellent anti-inflammatory capacity, antibacterial performance and biocompatibility. Interestingly, we found that trivalent chromium nanoparticles (NanoCr) showed both SOD-like and CAT-like activity and had excellent characteristics in a series of experiments on pulpitis. Subsequently, we further explored the potential of NanoCr as a capping or lining material in pulpitis treatment through a series of morphological and genetic studies, such as scanning electron microscopy and RNA sequencing (RNA-seq). Nanoparticles clearly enhanced the uptake of metal ions by dental pulp cells and continuously released chromium ions in the cells. At the cellular level, we found that NanoCr significantly reduced the production of inflammatory factors in pulpitis cells and reduced the excessive immune effect induced by

 

microbial infection. In addition, NanoCr had obvious antibacterial effects on *Escherichia coli*, *Enterococcus faecalis*, and *Porphyromonas gingivalis*. Therefore, this study has clearly demonstrated that nanoparticles prepared from chromium ions can remove ROS and decrease pulpitis inflammation and have favorable antibacterial properties with great application prospects in the clinical treatment of pulpitis (Fig. 1).

## 2. Results and discussion

### 2.1. Metallic nanoparticles show stable physical and chemical properties

In this study, we developed dozens of metallic nanoparticles based on our previous study.[32] To guarantee the reliability and repeatability of the following experiments, we characterized the physical and chemical properties of these metallic nanoparticles. The results of dynamic light scattering showed that the sizes of these nanoparticles were 30–60 nm (Fig. 2B–E), consistent with the results of the transmission electron microscopy (TEM) analysis. The particle sizes measured by dynamic light scattering were slightly larger than those measured by TEM, mainly because of the hydrated particle size. The metallic nanoparticles showed potential and were in a dispersed and stable state. In addition, the metallic nanoparticles could be stored for two weeks at 4 °C with good stability.

The NanoCr was prepared following two steps, including a water-in-oil (w/o) emulsion droplet-confined precipitation reaction and a film dispersion method, which was simple and safe and did not require special equipment. The existing Cr nanoparticle synthesis methods include hydrothermal method, precipitation method, vapor phase condensation method and arc-discharge method.[33] High-temperature calcination, high voltage, and special instruments are often required in the process.[34]

### 2.2. Metallic nanoparticles that have an acceptable influence on the proliferation of DPSCs are sorted out

To identify the effects of nanoparticles on the proliferation of dental pulp stem cells (DPSCs), a CCK8 assay was carried out. DPSCs were treated with different concentrations of nanoparticles (10, 50, 100, and 200 μM) for 1, 3, 5, and 7 days (Fig. 2A and S2†). Untreated DPSCs were considered the control group. The CCK-8 assay showed that 10 μmol $L^{-1}$ NanoAg, NanoCr, iron nanoparticles (NanoFe), aluminum nanoparticles (NanoAl), and barium nanoparticles (NanoBa) had no obvious influence on the proliferation of DPSCs compared to the control ($P > 0.05$). The nanoparticles mentioned above at concentrations of 50, 100, and 200 μmol $L^{-1}$ slightly reduced the proliferation of DPSCs. Other nanoparticles considerably decreased the proliferation of DPSCs over time. To ensure the lowest influence of the nanoparticles on DPSCs, we chose a concentration of 10 μM to continue the following experiments. Moreover, according to our previous research,[35] it is difficult for metal ions to enter cells independently, and our metal ion nanostorage was conducive to improving the trans-

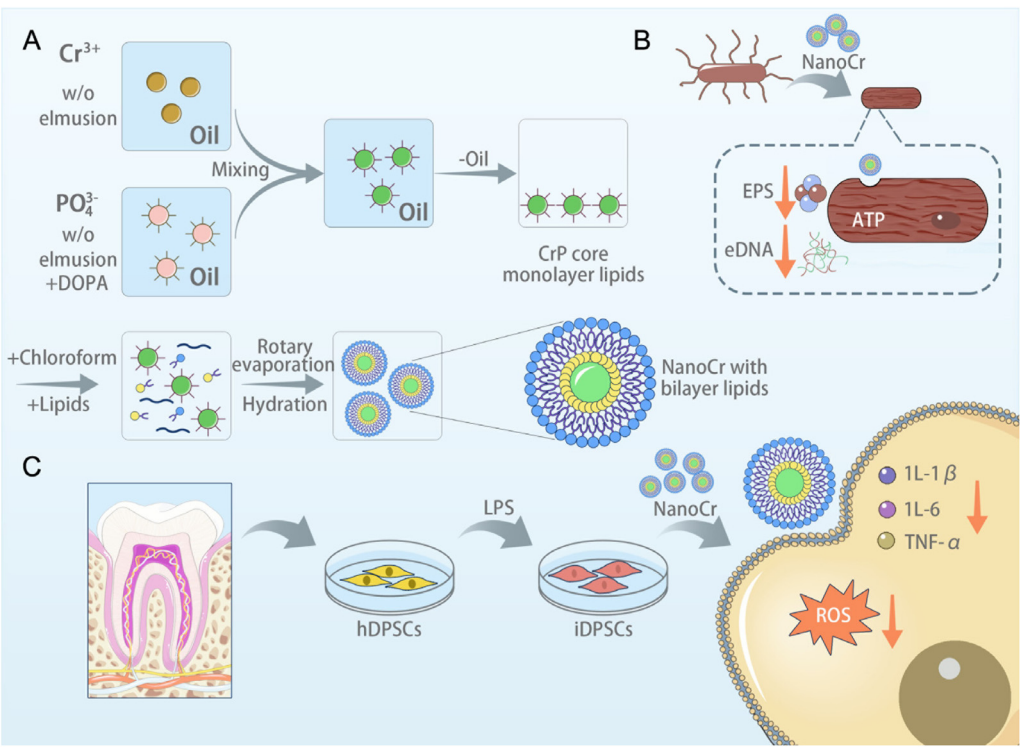


**Fig. 1** Schematic illustration of the synthesis and application of metal nanoparticles. (A) Schematic illustration showing the fabrication of NanoCr. (B) Antibacterial function of NanoCr. (C) Resources of DPSCs and the anti-inflammatory function of NanoCr on iDPSCs.

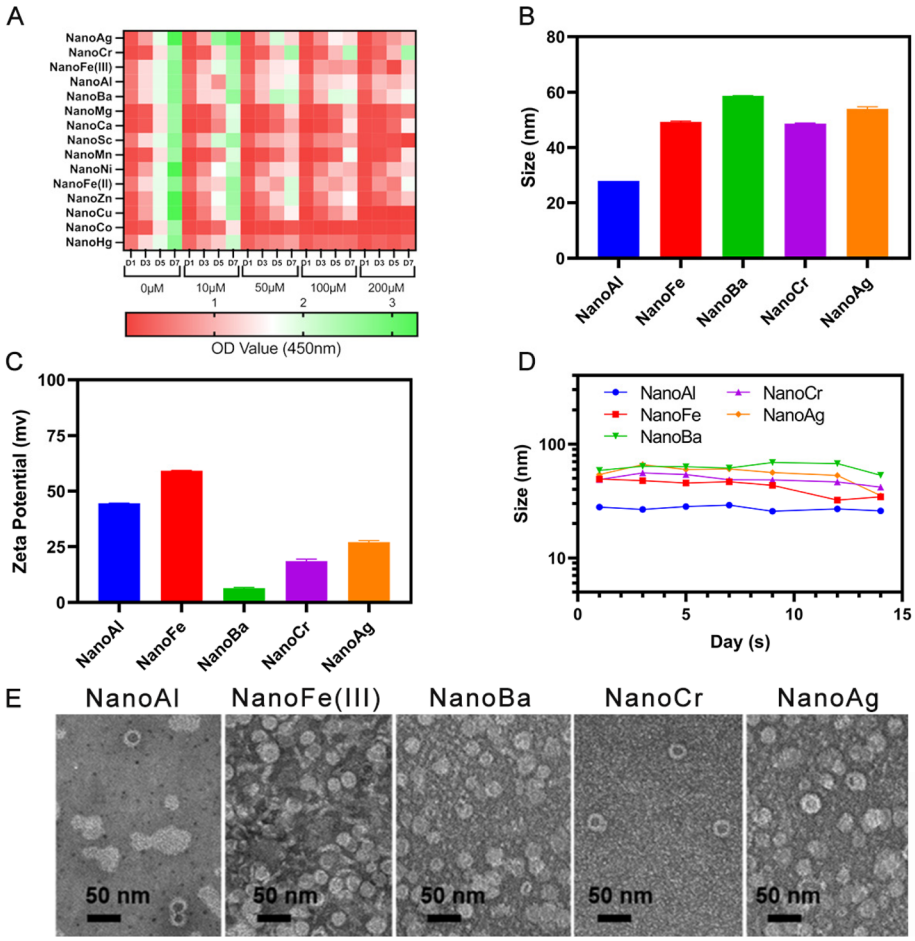


**Fig. 2** Characterization of nanoparticles. (A) Influence of 15 kinds of metal nanoparticles on the proliferation of DPSCs ($n$ = 3 per group). A CCK8 assay was carried out on days 1, 3, 5 and 7. (B) Size of metal nanoparticles ($n$ = 3 per group). (C) Zeta potential of metal nanoparticles ($n$ = 3 per group). (D) Experiment on the particle size stability of metal nanoparticles. (E) TEM images of 5 metal nanoparticles (scale bar: 50 nm).

port of metal ions into cells. Therefore, the use of metallic nanoparticles is advantageous for the treatment of pulpitis.

### 2.3. NanoCr is capable of reducing inflammatory factors

To isolate nanoparticles with a favorable anti-inflammatory ability, we utilized different methods, such as qPCR and ELISA, to detect the levels of inflammatory factors in cells of different administration groups. According to the qPCR results, the relative mRNA expression levels of the inflammatory cytokines IL-1β, IL-6 and TNF-α in inflamed dental pulp stem cells (iDPSCs) showed a significant increase after treatment with LPS for 3 h, which was the most obvious compared to 1 h and 6 h ($p$ < 0.001) (Fig. 3A–C and S3†). Both inflamed groups cultured with and without nanoparticles showed an increase in the expression levels of IL-1β, IL-6, and TNF-α after 3 h. Comparing different treatment groups, the expression levels were markedly decreased after treatment with NanoCr and NanoBa. Moreover, the expression levels of IL-1β and TNF-α were downregulated after treatment with NanoFe and NanoAg. However, IL-6 did not show a significant difference. NanoAl increased the expression of IL-1β after coincubation with iDPSCs (Fig. 3D–F). Similar results were observed by ELISA. NanoCr decreased the protein levels of all three inflammatory cytokines ($p$ < 0.05). NanoAg, NanoFe, and NanoBa decreased the protein levels of IL-1β and TNF-α but did not obviously influence that of IL-6, while NanoAl did not influence any of these three cytokines (Fig. 3G–I).

Dental pulp consists of defense cells and inflammatory mediators that regulate the response to infection. The upregulation of inflammatory cytokines such as IL-1β, IL-6, interleukin 10 (IL-10) and TNF-α has been observed in pulp cells in many previous studies.[36–38] Moreover, the TNF-α protein can induce neutrophil chemotaxis and activation. TNF-α is produced by activated macrophages, which play a fundamental role in early adaptive immune responses.[39] IL-6 is a pleomorphic cytokine related to processes involving the response to trauma and infection. IL-1β is a key cytokine involved in the mediation of inflammation and bone resorption.[40] In this study, NanoCr was found to reduce the inflammatory response by downregulating the expression of IL-1β, IL-6 and TNF-α.

The results indicated the potent effect of NanoCr on suppressing inflammatory cytokines that are involved in pulpitis, which is beneficial for the repair of pulp tissues.

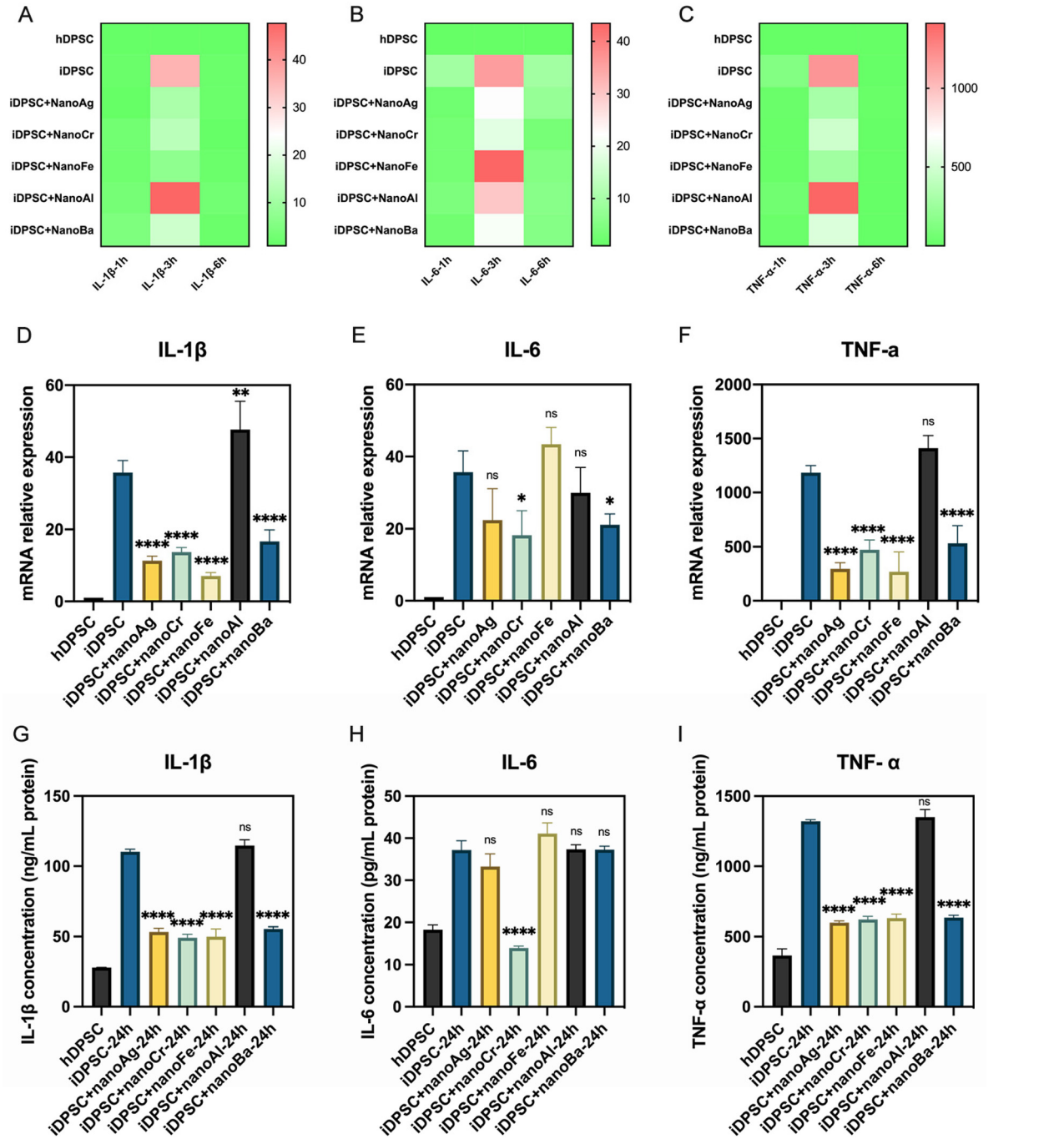


**Fig. 3** Anti-inflammatory properties of metal nanoparticles. (A–C) The expression of inflammatory cytokines (IL-1β, IL-6 and TNF-α) in DPSCs after treatment with nanoparticles for 1, 3 and 6 hours. (D and E) The expression of inflammatory cytokines (IL-1β, IL-6 and TNF-α) in DPSCs after treatment with nanoparticles was measured by RT-qPCR. (G–I) The expression of inflammatory cytokines (IL-1β, IL-6 and TNF-α) in DPSCs after treatment with nanoparticles was measured by ELISA. The values of *P* were measured in iDPSCs cultured with and without nanoparticles.

### 2.4. NanoAg, NanoCr and NanoBa show different degrees of antibacterial properties

Based on the above research, we continued to explore the antibacterial properties of the metallic nanoparticles. To demonstrate the antibacterial ability of these five metallic nanoparticles, we selected common oral pathogenic bacteria, including *E. coli, E. faecalis, and P. gingivalis*, for verification.

The bacterial growth curve indicates that NanoAg had a strong inhibitory effect on *E. coli* within 14 h of incubation, while the other metallic nanoparticles had a clear inhibitory effect on *E. coli*. When nanoparticles were co-incubated with *E. faecalis*, NanoCr had a significant antibacterial effect at 6 h.

When nanoparticles were co-incubated with *P. gingivalis*, NanoCr and NanoBa strongly inhibited the growth of bacteria during coincubation for up to 3 days (Fig. S4†).

The antibacterial results indicated that these five types of metallic nanoparticles exerted antibacterial effects on common oral pathogenic bacteria to different degrees. Compared with the control group, NanoAg had the most obvious antibacterial effect on *E. coli*, while NanoCr had the most obvious effect on *E. faecalis* and *P. gingivalis*. NanoBa had the best antibacterial effect on *P. gingivalis* (Fig. 4A–D). Among the nanoparticles, NanoFe and NanoAl had relatively poor antibacterial effects. Overall, the bacterial growth of *E. coli*, *E. faecalis*, and *P. gingivalis* was significantly inhibited by NanoCr.

Antibacterial properties are considered of great importance for dental materials. Moreover, *E. faecalis* is considered the main microorganism associated with endodontic failure.[41] Additionally, the expression of inflammatory cytokines can be upregulated after stimulation with LPS from *E. coli.*[5] Furthermore, *P. gingivalis* has been suggested to exist in all phases of endodontic retreatment.[42] This study showed the antibacterial properties of NanoCr toward these three organisms, which could be a considerable advantage for its application in dental materials.

Through the results above, we isolated NanoCr, which has suitable biosafety and superior antibacterial and anti-inflammatory functions. Next, we carried out experiments to further explore the underlying mechanisms of the antibacterial and anti-inflammatory functions of NanoCr.

### 2.5. Uptake of NanoCr into DPSCs is efficient and relative to time

To further characterize NanoCr in detail, we used an element analyzer to detect the elemental composition of the nanoparticles. NanoCr contains phosphorus and chromium (Fig. S1†). To verify the uptake efficiency of NanoCr by DPSCs, the nanoparticles were incubated for different times and then analyzed qualitatively and quantitatively by inductively coupled plasma-mass spectrometry (ICP-MS) and fluorescence microscopy (Fig. 5A and Fig. S5†). The efficiency of NanoCr uptake by cells was approximately 10% within 24 hours, and the content of chromium ions was 150 ng at 24 hours. With increasing incubation time, the content of chromium ions in cells increased gradually (Fig. 5B and C). Therefore, DPSCs can effectively absorb NanoCr, and the efficiency of cell uptake of nanoparticles gradually improves over time.

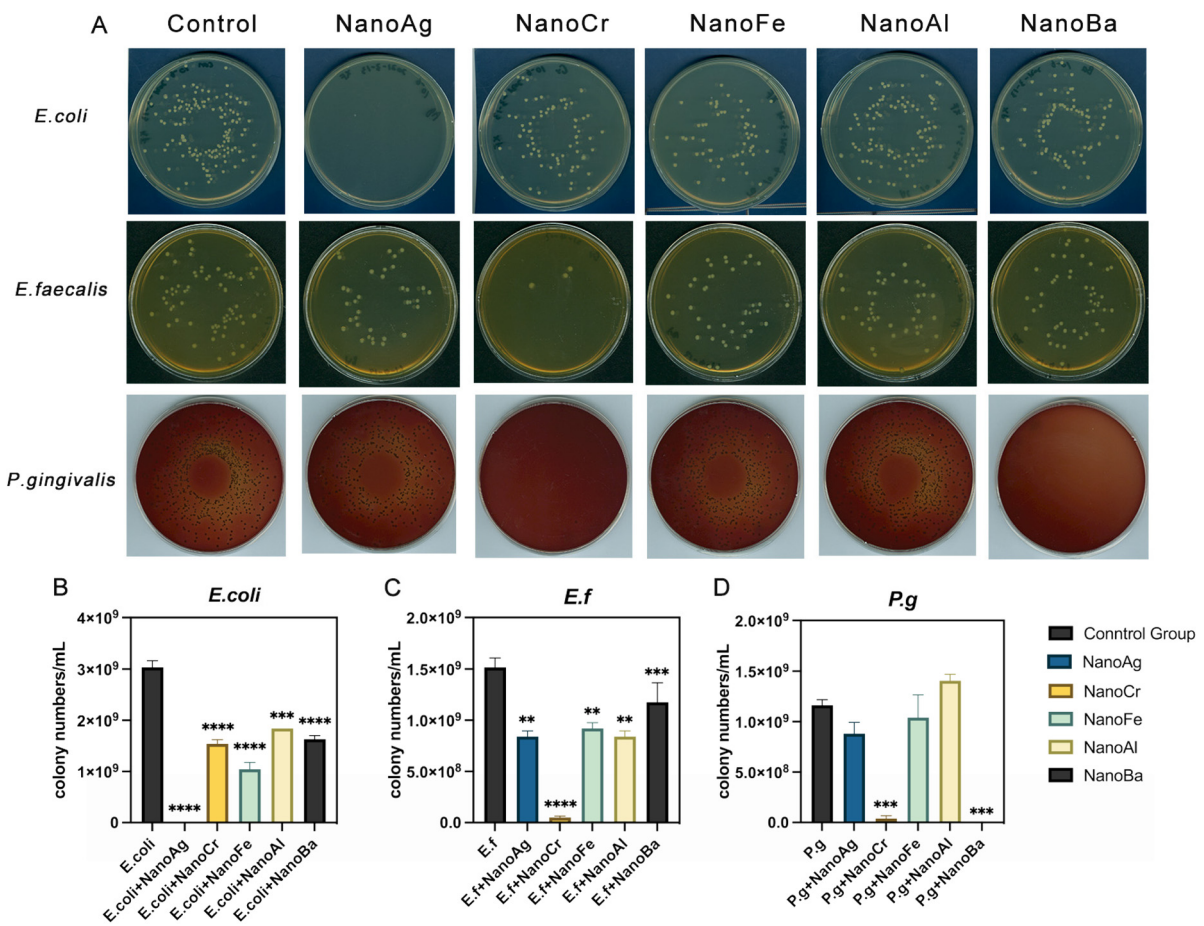


Fig. 4 Antibacterial properties of metal nanoparticles. (A) *E. coli, E.f.* and *P. gingivalis* colonies grown on agar plates after treatment with different nanoparticles. (B and D) Colony number analysis of *E. coli, E. f* and *P. gingivalis* ($n$ = 3 per group).

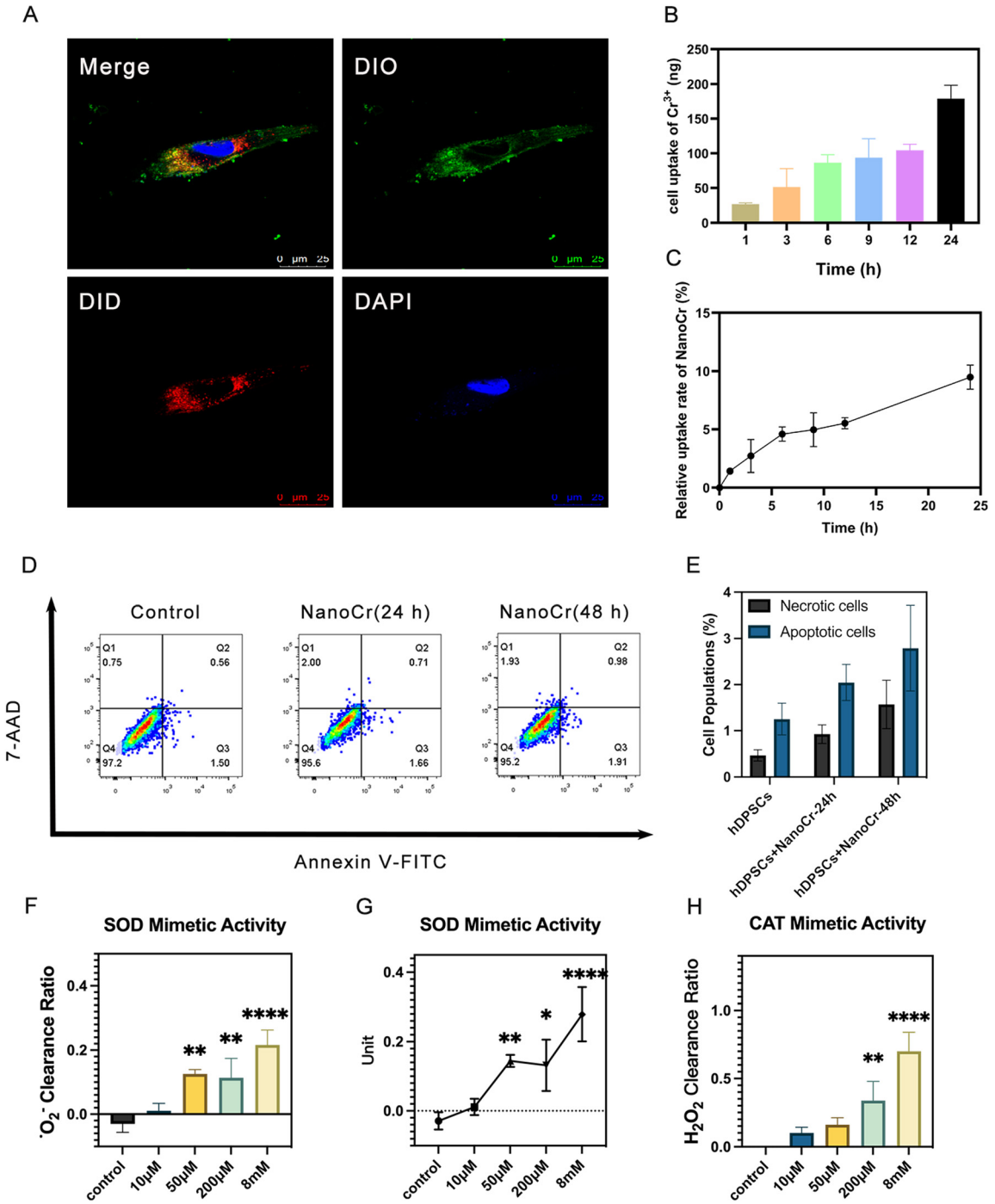


**Fig. 5** Cellular uptake, cell apoptosis and enzyme-mimetic ROS scavenging capacity of NanoCr. (A) The results of DPSC uptake of DID-labeled NanoCr observed by confocal microscope (incubation time: 6 h; DID labeling nanoparticles, DAPI labeling nuclei, and DIO labeling cell membranes). (B and C) Quantitative analysis of the efficiency of dental pulp cells in the uptake of NanoCr (10 μM) and the content of chromium ions at different time points ($n$ = 3 per group). (D) Flow cytometry analysis of DPSCs after treatment with NanoCr (10 μM) for 24 and 48 hours ($n$ = 3 per group). (E) Cell population analysis of different cell stages according to flow cytometry analysis. (F) Enzyme-mimetic capacity of NanoCr showing in $^{\cdot}O_2^-$ clearance ratio. (G) SOD mimetic activity of NanoCr. (H) $H_2O_2$ clearance ratio of NanoCr showing its CAT mimetic activity.

NanoCr is a microprecipitation of chromium phosphate encapsulated in liposomes, which undergoes responsive disintegration under an acidic environment in inflammatory cells. In addition, sustained release of chromium ions within the cytoplasm was achieved. However, some of the reported nano chromium materials are stable in the aforementioned pH environment and are not suitable for biological experiments and treatments.[43]

### 2.6. NanoCr has little effect on cellular apoptosis of DPSCs

Subsequently, we verified the toxicity of NanoCr by apoptosis assays. Apoptosis of NanoCr on DPSCs was investigated using Annexin V-FITC/PI staining (Fig. 5D). DPSCs treated with NanoCr remained mostly viable compared with untreated DPSCs, as indicated by Annexin V-FITC/PI staining (Fig. 5D and E). The population of apoptotic cells was slightly increased after 48 h of coculture with NanoCr compared to that at 24 h (Fig. 5D and E), indicating that NanoCr had little effect on apoptosis induction in DPSCs. Combined with the previous cytotoxicity experiments of NanoCr, it can be concluded that NanoCr is safe for use on DPSCs.

Liposome nanoparticles have good cell compatibility. They are drug formulations approved by the Food and Drug Administration (FDA) that have great potential for clinical application.[44]Toxicity induced by nanoparticles has always been a major concern in the biomedical application of nanoparticles. Extensive use of nanoparticles may lead to toxicity in human beings and the environment.[45] The main intake pathways of nanoparticles include exposure through inhalation, dermal contact, or ingestion.[46] The principal mechanism of nanoparticle toxicity involves ROS and free radical production.[47] Horie *et al.* indicated an increase in intracellular ROS levels and activation of antioxidant defense systems after exposure to $Cr_2O_3$ nanoparticles. Their research showed that the decrease in cell viability by exposure to $Cr_2O_3$ nanoparticles was caused by apoptosis.[48] However, most existing studies on the cytotoxicity of nanoparticles have focused on *in vitro* cell culture. NanoCr was mainly applied locally for the treatment of pulpitis in this research; thus, its systemic effects were limited. In general, our findings indicate that NanoCr has application potential in the treatment of oral pulpitis.

### 2.7. NanoCr is capable of mimicking intracellular enzymes in scavenging $^{\cdot}O_2^-$ and $H_2O_2$

In this study, ROS-scavenging capacity and antioxidant enzyme-like capacity were evaluated. First, NanoCr exhibits SOD-mimetic capacity by catalyzing $^{\cdot}O_2^-$, which was detected by WST-8. The inhibition ratio reached 21.6% at a concentration of 8 mM (Fig. 5F), while the SOD mimetic activity was 0.28 units (Fig. 5G). The CAT-like capacity was determined by the $H_2O_2$-specific probe xylenol orange. The clearance ratio of $H_2O_2$ increased from 33.8% at 200 μM to 70.1% at 8 mM with increasing concentrations of NanoCr (Fig. 5H). Deionized water, a dissolvent of NanoCr, was selected as the negative control in the experiments. The results above showed the antioxidative enzyme-like capacity of NanoCr, which can be used for treating ROS-related inflammatory diseases, including pulpitis.

### 2.8. NanoCr mediates the expression of genes related to inflammation in DPSCs

To investigate the mechanism underlying the anti-inflammatory effects of NanoCr on DPSCs, mRNA sequencing was carried out to compare the gene expression of untreated DPSCs and DPSCs cultured with NanoCr.

The differentially expressed genes were analyzed, and the corresponding heatmap was depicted to display the up and downregulated genes between three groups (Fig. 6A). DEGs in DPSCs cultured with and without NanoCr are presented in the volcano plot, which shows the upregulated expression of 200 genes and downregulated expression of 99 genes (Fig. 6C). Then, the DEGs were subjected to Gene Ontology (GO) analysis, by which they were classified into molecular function, cellular component, and biological process categories. The GO database analysis showed that DEGs related to the inflammatory response (23 genes), immune response (16 genes) and cellular response to lipopolysaccharide (16 genes) were among the most enriched DEGs, which indicated changes in inflammation-associated biological processes. Furthermore, Kyoto Encyclopedia of Genes and Genomes (KEGG) pathway investigation was executed to reveal the potential biological processes and identify the molecular pathways involved. As shown in Fig. 6D, the TNF signaling pathway, NF-kappa B signaling pathway, MAPK signaling pathway, and IL-17 signaling pathway were among the most enriched pathways. The NF-κB pathway has long been considered a prototypical proinflammatory signaling pathway.[49] In most inflammatory cells, MAPK is activated and crucial to inflammatory cytokine production and signaling.[50] The analysis of the other two categories is included in the ESI (Fig. S6†). These results indicated that NanoCr could mediate the expression of inflammation-related genes, possibly through the NF-kappa B and MAPK pathways.

### 2.9. NanoCr downregulates inflammatory activity *via* the NF-kappa B and MAPK signaling pathways

To further explore the anti-inflammatory properties of NanoCr, we measured the ROS levels in DPSCs with and without NanoCr treatment (Fig. 7A and B). The LPS-induced inflammatory cell model triggered the production of much ROS (Fig. 7A and B). Moreover, the expression levels were significantly lowered after treatment with NanoCr ($p < 0.05$) (Fig. 7A and B).

ROS are also key signaling molecules that play an important role in the progression of inflammatory disorders because they oxidize protein and lipid cellular constituents and damage DNA.[51] ROS play an important role in translating the binding of extracellular receptors into functional transcription, which has been implicated in multiple signaling cascades, including the MAPK/ERK and NF-kappa B pathways.[52] ROS-mediated activation of NF-κB may result in the production of IL-6, TNFα and IL-1α/β,[53] which is also consistent with our previous results. Many reports have indicated that MAPKs play important roles in several biological processes, such as responses to stress and inflammation.[54] Inhibition of the MAPK or NF-kappa B signaling pathway has been indicated to be a successful method for reducing inflammatory activity.

To further elucidate the mechanism underlying the inhibitory effect of NanoCr on inflammatory cytokine secretion, we investigated the effect of NanoCr intervention on the activation of the NF-kappa B and MAPK signaling pathways. LPS significantly increased the activation of NF-kappa B and MAPK by increasing the phosphorylation of p65, p38 and pERK1/2

 

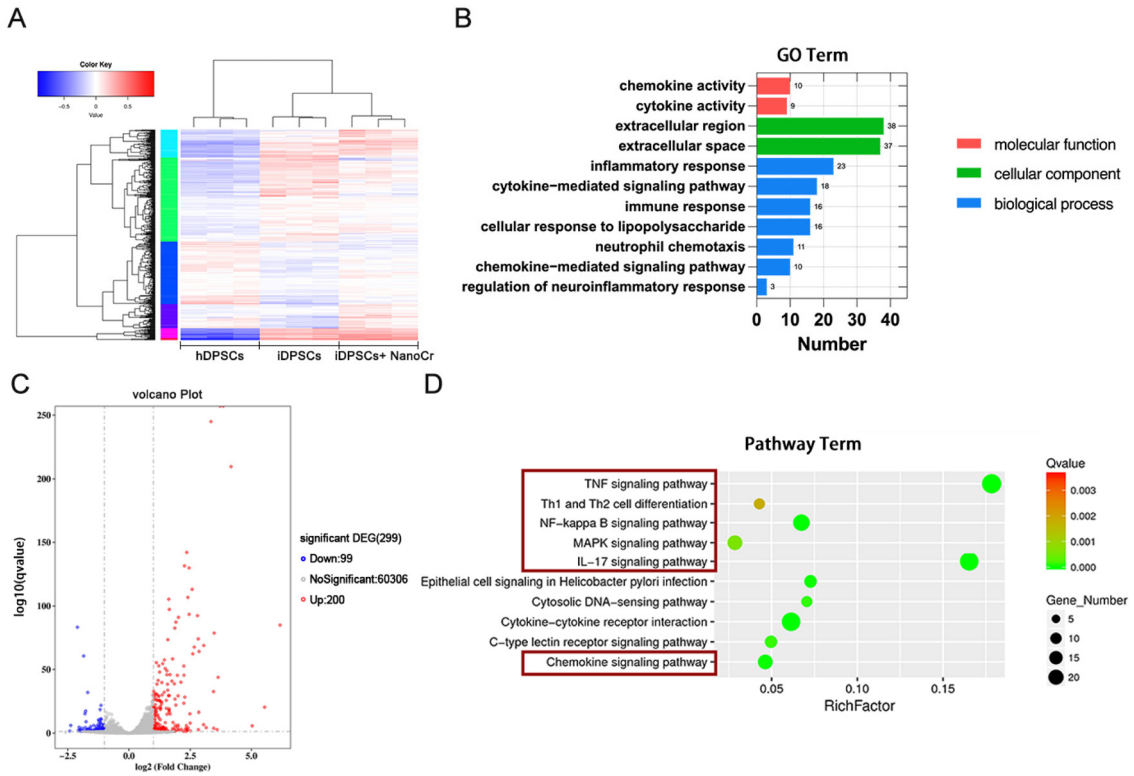


**Fig. 6** mRNA sequencing results of DPSCs treated with and without NanoCr. (A) Clustered heatmap of differentially expressed genes depicting the up (red) and downregulated (blue) genes in hDPSCs, iDPSCs, and iDPSCs cultured with NanoCr. (B) GO term enrichment of DEGs. (C) Volcano map of genes that were significantly upregulated (red dots), downregulated (blue) and not significantly changed (gray) (hDPSCs *vs.* iDPSCs cultured with NanoCr). (D) KEGG pathway enrichment analysis of DEGs.

(Fig. 7C and D). NanoCr efficiently suppressed the phosphorylation of p65, p38 and pERK1/2 (Fig. 7C and D), indicating that NanoCr likely inactivated the NF-kappa B and MAPK pathways. Overall, NanoCr promoted the inactivation of the NF-kappa B and MAPK signaling pathways, which is the mechanism of its anti-inflammatory function.

### 2.10. NanoCr prohibits the proliferation of *E. coli* by interfering with its metabolic progress

Transcriptome sequencing of *E. coli* was carried out to further explore the mechanism underlying the antibacterial properties of NanoCr. The volcano plot shows the differential expression of genes between *E. coli* with or without NanoCr treatment (Fig. 8A). Altogether, 16 genes were downregulated. GO analysis indicated the enrichment of genes in processes related to metabolism and transmembrane transport, such as proton-transporting ATP synthase activity, C4-dicaboxylate transmembrane transporter activity, and ATP synthesis-coupled proton transport (Fig. 8B).

KEGG pathway analysis showed that the DEGs were enriched mainly in 6 pathways, such as oxidative phosphorylation and metabolic pathways, which are related to the cell metabolism of *E. coli* (Fig. 8C). For example, the ABC transporter is a transport ATPase located on the bacterial membrane that plays an important role in the uptake of micronutrients into bacteria. Flagella assembly is also among the most enriched pathways (Fig. 8C), which is one of the central systems responsible for bacterial motility. Bacterial cells sense changes in the environment and migrate toward more desirable locations through flagella-driven motility.[55] The results indicated that NanoCr also has an influence on the structure of bacteria.

In general, these results indicated that the antibacterial properties of NanoCr are mediated through interference with the metabolism and transmembrane transport of bacteria. A clustered heatmap and cluster of orthologous groups (COG) distribution map are provided in the ESI (Fig. S7†).

### 2.11. NanoCr can damage the pathogenic structure of bacteria and lower the ATP level in their cells

To further explore the effect of NanoCr on *E. coli, E. faecalis* and *P. gingivalis*, we used SEM to observe the morphological changes in these microorganisms after treatment with NanoCr. The morphology of *E. coli* cells was regular, and flagella were intact before coculture with NanoCr. *E. coli* cells grown in culture medium with 10 μg $mL^{-1}$ NanoCr appeared to be damaged, with a shriveled surface and cracked flagella. Moreover, untreated *P. gingivalis* cells were plump and surrounded by extracellular matrix. After treatment with NanoCr, the *P. gingivalis* cells became atrophic, and the extracellular

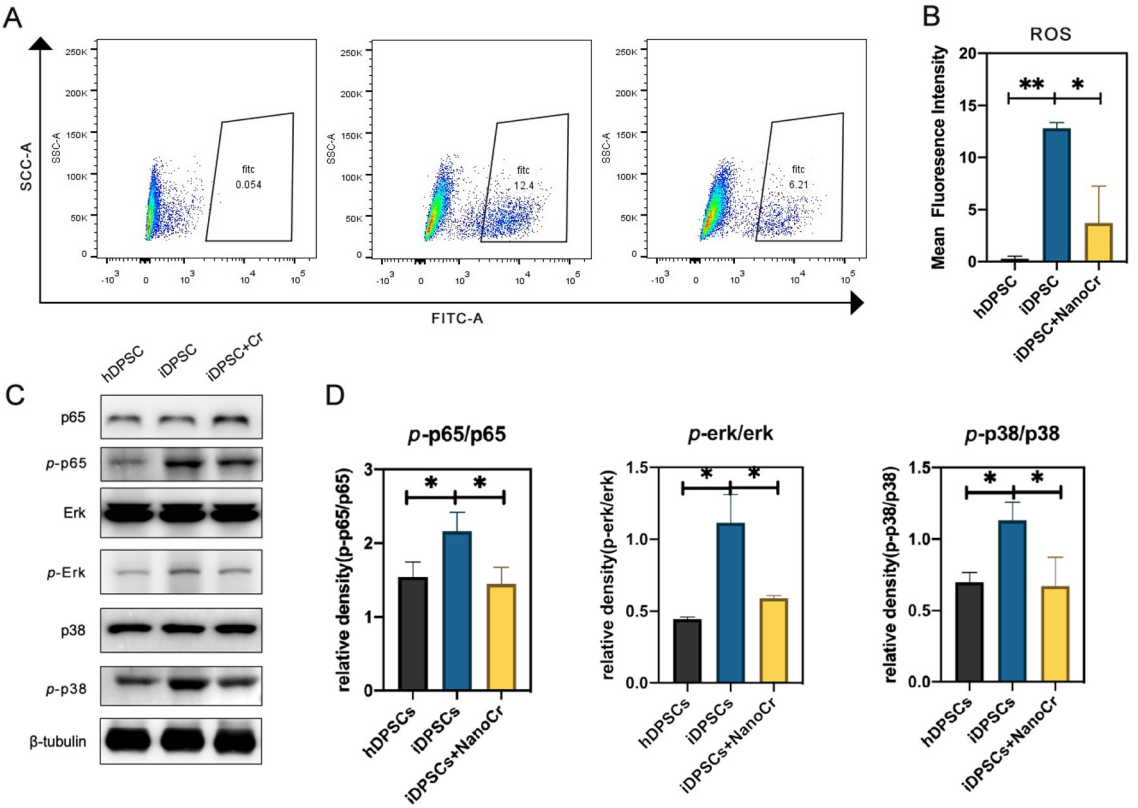


**Fig. 7** Mechanism underlying the anti-inflammatory properties of NanoCr. (A and B) Flow cytometry analysis of ROS produced by DPSCs treated with or without NanoCr and mean fluorescence intensity analysis. (C) Western blot analysis of the expression of proteins in the NF-κB and MAPK signaling pathways (Erk1/2, p65 and p38). (D) Analysis of the density of bands using ImageJ.

matrix almost completely vanished. However, no obvious differences were observed in the appearance of *E. faecalis* (Fig. 8F). Moreover, the ATP level of all microorganisms in culture media was significantly reduced after treatment with 10 μg $mL^{-1}$ NanoCr ($p < 0.001$) (Fig. 8E). Additionally, the distribution of NanoCr was determined by SEM-EDS elemental mapping, which showed that Cr and P ions were uniformly distributed in the bacteria (Fig. 8D and S8†).

The bacterial flagellum Is a helical filamentous organelle responsible for motility, which can be a crucial factor in the virulence of pathogenic bacteria.[56,57] Bacterial flagellar motility plays an important role throughout infection, including adhesion and biofilm formation.[58,59] Our results showed that NanoCr destroyed the flagella of *E. coli*, thus decreasing its pathogenicity. Moreover, the biofilm extracellular matrix of *P. gingivalis* is composed mainly of extracellular polysaccharides (EPS), proteins, lipids, and extracellular DNA.[60] These components play important roles in cell adhesion, aggregation, cohesion and structural integrity during biofilm formation and development and act as protective barriers against *P. gingivalis*.[61] NanoCr reduced the activity of *P. gingivalis* and therefore decreased the secretion of extracellular matrix, which could interfere with the formation of biofilms on the dental surface. Additionally, *E. faecalis* is a facultative anaerobic Gram-positive bacterium whose bacterial cell wall serves as a protective cellular barrier. Our results did not show NanoCr destroying the cell wall of *E. faecalis*. However, its main underlying mechanism of antibacterial function could be the downregulation of the ATP level, as NanoCr reduced the activity of the microorganisms. Apart from the production of ROS mentioned before, the mechanism underlying the bactericidal effect of nanoparticles could be mediated through attachment to the surface of the cell membrane and disrupting its proper function or penetrating into the bacterial cell, causing further damage and releasing metal ions.[62] Overall, the mechanisms underlying the antibacterial properties of NanoCr still need further exploration.

Although we have demonstrated that NanoCr has significant effects in inhibiting inflammation, clearing ROS, and antibacterial ability, there is still room for improvement. Although chromium ions have excellent compatibility with DPSCs in the form of liposome nanoparticles, they cannot be directly used for the treatment of pulpitis in colloidal solution.

For further clinical application, a stable form is necessary. For example, after mixing with excipients such as gel and biological scaffolds, NanoCr can be injected into pulp cavities to become a good lining material. Chromium ions can be slowly released to achieve long-term effective antibacterial and anti-inflammatory therapeutic effects. In addition, NanoCr can also be made into paint-coat, which can be applied on dental

 

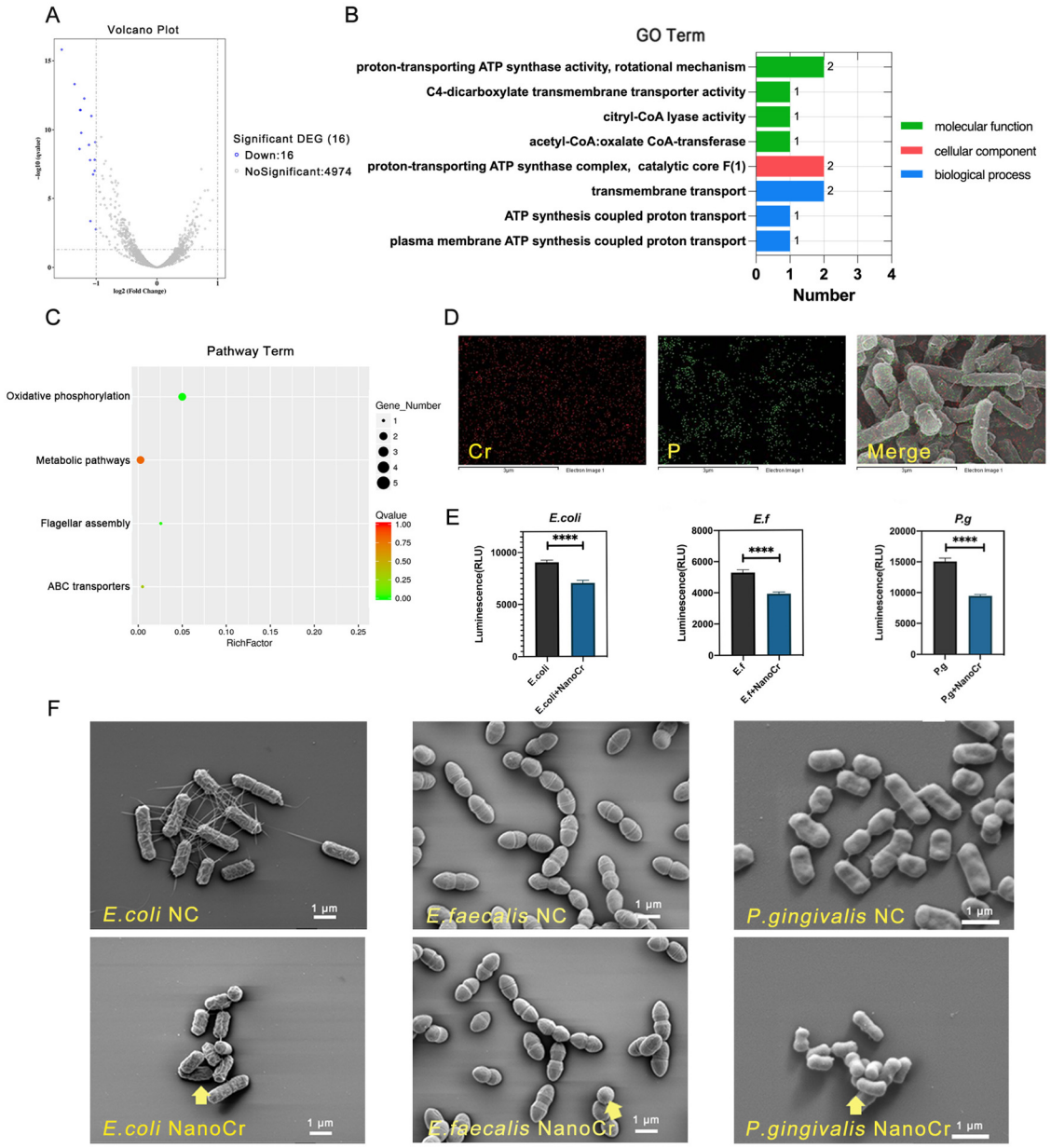


**Fig. 8** Mechanism of the antibacterial properties of NanoCr. (A) Volcano map of genes that are significantly downregulated (blue dots) and insignificantly changed (gray dots). (B) GO term enrichment of DEGs. (C) KEGG pathway enrichment analysis of DEGs. (D) EDS images of *E. coli, E. f* and *P. gingivalis*. (E) ATP level of the culture medium of *E. coli, E. f* and *P. gingivalis*. (F) SEM images of *E. coli, E. f* and *P. gingivalis*. Arrows represent the changes in bacteria after incubation with nanoparticles.

equipment, for instance, dental implants, to reduce the risk of postoperative infection and inflammation. We will pay more attention to the clinical conversion of NanoCr in our future research.

## 3. Conclusions

In this study, we designed and constructed a standardized metallic nanoparticle synthesis platform and prepared a series of metallic nanoparticles with core–shell structures, among which NanoCr was selected due to its potential for pulpitis treatment. A series of investigations were performed in this study to improve our understanding of the antioxidative effect of NanoCr and its mechanisms. *In vitro* experiments suggested that NanoCr exhibited satisfactory ROS removal ability, indicating its potential as an ROS scavenger. NanoCr also had good biocompatibility. It had little influence on cell proliferation and cellular apoptosis at a concentration of 10 μM and could be absorbed efficiently by DPSCs. Using an inflammatory cell model, we further authenticated the ROS removal ability and anti-inflammatory activity of NanoCr, the mechanism of which

is by inhibiting MAPK and NF-kappa B pathway activation. Furthermore, NanoCr showed favorable antibacterial properties when cocultured with bacteria by damaging their cell membrane structures and interfering with their metabolic processes. Taken together, NanoCr exhibited SOD- and CAT-mimetic capacity and showed a fine balance between these properties, meeting the two main requirements of pulp capping materials. In the future, we will focus mainly on the effectiveness of NanoCr on pulpitis in a rat model and further explore its antibacterial properties in the oral cavity. In conclusion, NanoCr could be a promising material for pulp repair and an effective material for the treatment of pulpitis.

# 4. Experimental section

## 4.1. Materials and reagents

Barium chloride ($BaCl_2$), waterless ethanol, chromium chloride ($CrCl_3$), ferric chloride ($FeCl_3$), ferrous sulfate ($FeCl_2$), manganese chloride ($MnCl_2$), cyclohexane, magnesium chloride ($MgCl_2$), cobalt chloride ($CoCl_2$), mercurous chloride ($HgCl_2$), zinc chloride ($ZnCl_2$), copper chloride ($CuCl_2$), silver nitrate ($AgNO_3$), nickel chloride ($NiCl_2$), scandium chloride ($ScCl_2$), sodium aluminate ($NaAlO_2$), and calcium chloride ($CaCl_2$) were obtained from Beijing Tonguang. Potassium phosphate, disodium hydrogen phosphate, sodium dihydrogen phosphate, and phospholipids (DOTAP, DOPA and cholesterol) were ordered from Sigma-Aldrich. DSPE-$PEG_{2000}$, DiD and DiR were purchased from Shanghai Yuanye.

## 4.2. Synthesis and physicochemical properties of metallic nanoparticles

Nanoparticles were prepared according to our previous research.[32] Taking the preparation of NanoCr as an example, the volume ratio of the oil phase required for the first coordination reaction is cyclohexane/Igepal CO-520 (V/V = 70 : 30). A total of 15 mL of the oil phase was added to two centrifuge tubes. Then, 300 mL of the oil phase was added to two centrifuge tubes with 300 μL of potassium phosphate aqueous solution (25 mM), 300 μL of chromium chloride solution (500 mM) and 200 μL of DOPA (20 mg $mL^{-1}$) during the phosphate phase. The two oils were mixed by inversion several times and then allowed to stand for 20 min. Then, we added the same amount of absolute ethanol into the tube for demulsification and centrifuged at high speed (12 000*g*, 20 min) to obtain the final nanoprecipitate. After washing the precipitate with absolute ethanol several times, we added 100 μL of DSPE-$PEG_{2000}$ (3 mM) and 100 μL of DOTAP/cholesterol (molar ratio 1 : 1, 10 mM). Finally, we used the thin-film dispersion method to remove the organic solvent on the rotary evaporator. After the organic solvent was evaporated, the lipid membrane was dispersed in 800 μL of deionized water to form a uniform and translucent nanoparticle solution. Finally, the prepared nanomaterials were stably preserved at 4 °C.

The other nanoparticles were prepared using the same methodology described above except that the different metal ions were mixed with a phosphate solution of the corresponding valence, such as disodium hydrogen phosphate or sodium dihydrogen phosphate. TEM with energy dispersive X-ray spectrometry was used to examine the external form of nanoparticles and the spatial distribution of elements over them. The surface charge (zeta potential, mV) of the nanoparticles was measured by dynamic light scattering.

## 4.3. ROS scavenging activity assay

Scavenging of two kinds of ROS, $H_2O_2$ and $^{\bullet}O_2^-$, was evaluated to determine the ROS scavenging activity of NanoCr. The experiments were conducted according to the protocols of the assay kits. The $^{\bullet}O_2^-$ scavenging activity was determined with a Total Superoxide Dismutase Assay Kit (Beyotime, Shanghai, China). The $H_2O_2$ scavenging activity was evaluated with a Hydrogen Peroxide Assay Kit (Beyotime, Shanghai, China).

## 4.4. Cell culture

DPSCs were provided by ORAL STEM CELL BANK run by Beijing Tason Biotech. The cells were grown in α-modified minimum essential medium (α-MEM, Gibco/BRL, USA) supplemented with 10% fetal bovine serum (FBS, Gibco, USA), 100 U $mL^{-1}$ penicillin, and 100 μg $mL^{-1}$ streptomycin at 37 °C in 5% $CO_2$. DPSCs between the fourth and eighth passages were used for the following experiments.

## 4.5. Cell proliferation assay

The influence of nanoparticles on the proliferation of DPSCs was assessed with a CCK-8 assay. DPSCs were seeded in 96-well plates ($3 \times 10^3$ cells per well; expanded *ex vivo*) and treated with 0, 10, 50, 100, and 200 μmol $L^{-1}$ metallic nanoparticles. At 1, 3, 5, and 7 days after cell seeding, a CCK-8 (Dojindo, Japan) assay was carried out with three replicates to evaluate the number of viable cells.

## 4.6. Quantitative real-time PCR

DPSCs were treated with *Escherichia coli* lipopolysaccharide (LPS: 1 μg $mL^{-1}$) (Sigma Aldrich, St Louis, MO, USA) to induce an inflammatory reaction. iDPSCs were treated with 10 μmol $L^{-1}$ nanoparticles for 1 h, 3 h and 6 h. The relative expression level of inflammatory cytokines was measured by quantitative real-time PCR. Interleukin 1 beta (IL-1β), interleukin 6 (IL-6), and tumor necrosis factor-α (TNF-α) primers were used to assess inflammation expression levels in DPSC mRNA. All primers are listed from 5′ to 3′. GAPDH was used as a housekeeping gene to normalize the data obtained from the RT-qPCR and calculate the relative fold change between conditions. qPCR was carried out using SYBR Green master mix (Roche, Indianapolis, IN, USA) with 0.5 μL of cDNA and 200 nM specific primers. The thermal cycling parameters were as follows: 50 °C for 2 min and 95 °C for 10 min, followed by 40 cycles at 94 °C for 15 s and 60 °C for 1 min. An ABI PRISM 7500 Sequence Detection System (Applied Biosystems, Foster City, CA, USA) was used.

 

### 4.7. ELISA

DPSCs were treated with 1 μg $mL^{-1}$ LPS in the presence of 10 μmol $L^{-1}$ nanoparticles for 24 h. The protein levels of IL-1β, IL-6 and TNF-α in the iDPSC medium were determined by ELISA kits (Meimian, Jiangsu, China) according to the instructions. Reference solutions of the inflammatory cytokines were first diluted to 6 standards at concentrations of 0, 25, 50, 100, 200, and 400 ng $mL^{-1}$ to establish a standard curve. Then, the standards and test samples were added to a 96-well plate precoated with the antibody. The plate was incubated for 30 min at 37 °C and then washed 5 times using washing buffer. Avidin-HRP was added and incubated for 30 min, followed by 5 washes. Finally, TMB substrate was added and incubated for 10 min. The absorbance at 450 nm wavelength was recorded within 15 min by a microplate reader after the stop solution was added. The protein levels of the inflammatory cytokines were then calculated according to the standard curve.

### 4.8. mRNA sequencing of NanoCr-treated DPSCs

DPSCs cultured in 6-well plates were treated with 1 μg $mL^{-1}$ LPS with and without 10 μM NanoCr for 3 h. Total mRNAs were extracted from the DPSC treatment groups. Then, transcriptome sequencing was performed by Azenta Life Sciences (Nanjing, China).

### 4.9. Qualitative and quantitative analysis of cellular uptake of NanoCr

DPSCs were cultured in α-MEM at 37 °C overnight. To detect the cellular uptake of NanoCr, cells were incubated with NanoCr-DiD in confocal dishes at different time points. Then, the cells were washed with fresh PBS twice and incubated with Hoechst 33342 and Lyso-Tracker Green for 10 min at 37 °C. DPSCs were washed again with PBS and observed with confocal laser scanning microscopy (CLSM).

In addition, ICP-MS was used to quantitatively detect the uptake efficiency of nanoparticles. DPSCs were treated with 10 μmol $L^{-1}$ NanoCr at different time points (0 h, 1 h, 3 h, 6 h, 9 h, 12 h, and 24 h) and then washed with PBS to remove unabsorbed NanoCr. DPSCs were then digested with trypsin without EDTA and collected after centrifugation (5 min, 1000 rpm). The chromium ion content of each sample and initial solution was detected by ICP-MS. The content of chromium ions in the actual cells measured by ICP was statistically plotted at different time points to obtain the content of chromium ions absorbed by the cells. Then, based on the actual uptake of chromium ions by cells and the content of chromium ions in the same dose of NanoCr raw samples at the time of administration, the relative uptake rate can be obtained through analysis. The formula for calculating the relative uptake rate of NanoCr is as follows:

$$\text{Relative uptake rate of NanoCr}(\%) = \frac{\text{Content of chromium ions in cell samples}}{\text{Content of chromium ions in the same dose of NanoCr}}$$

### 4.10. Cell apoptosis analysis of NanoCr

Apoptotic cell death of DPSCs induced by NanoCr was measured by flow cytometry analysis of Annexin V-FITC and PI staining. DPSCs ($3 \times 10^5$) were seeded in 6-well plates and incubated at 37 °C for 24 h and 48 h. Then, the cells were treated with 10 μmol $L^{-1}$ NanoCr. After 24 h and 48 h of incubation, the cells were washed with PBS, trypsinized, and collected by centrifugation. Then, DPSCs were resuspended in Annexin V binding buffer solution. The cells were stained according to the manufacturer's protocol (Solarbio, Beijing, China). The fluorescence intensities of Annexin V and PI staining were measured using a flow cytometer (FACS Calibur, BD Biosciences).

### 4.11. Detection of ROS

Quantitation of ROS was detected with an ROS assay kit (Beyotime, Shanghai, China) according to the manufacturer's protocol. DPSCs in 6-well plates were treated with 1 μg $mL^{-1}$ LPS in the presence of 10 μmol $L^{-1}$ NanoCr for 3 h. Then, 1 mL of 10 μmol $L^{-1}$ DCFH-DA was added to each well. The cells were cultured for 20 min at 37 °C, washed with PBS, and then measured using a flow cytometer (FACS Calibur, BD Biosciences).

### 4.12. Western blot

DPSCs were seeded into 6-well plates and treated with 1 μg $mL^{-1}$ LPS with and without NanoCr for 3 hours. DPSCs were lysed in RIPA buffer with protease inhibitors. Proteins were quantified by BCA Protein Assay (Thermo, USA). Thirty micrograms of protein from each sample was separated on 10% SDS-PAGE gels and transferred to PVDF membranes at 100 mA for 110 min. The membranes were bathed in blocking buffer (5% nonfat dry milk or bovine serum albumin in Tris-buffered saline with 0.05% Tween-20, pH 7.4) for 1 h and then incubated with the following antibodies at 4 °C overnight: p65 (K200045 M, Solarbio), phosphorylated p65 (K006216P, Solarbio), p38 (A4771, Abclonal), phosphorylated p38 (AP0057, Abclonal), Erk1/2 (A4782, Abclonal), phosphorylated Erk1/2 (AP0485, Abclonal) and β-tubulin (Solarbio). The membranes were incubated in horseradish peroxidase-conjugated secondary antibody (Solarbio) for 1 h at room temperature, and bands were visualized using BeyoImager™ 600.

### 4.13. Antibacterial assay

The antibacterial activity of the nanoparticles was evaluated by the bacterial counting method using *Escherichia coli* (ATCC25922) (*E. coli*), *Enterococcus faecalis* (CGMCC1.2135) (*E. faecalis*), and *Porphyromonas gingivalis* (ATCC33277) (*P. gingivalis*). A solution containing bacteria at a concentration of $10^6$ CFU $mL^{-1}$ *E. coli*, $10^5$ CFU $mL^{-1}$ *E. faecalis* or $10^5$ CFU $mL^{-1}$ *P. gingivalis* was mixed with 10 μmol $L^{-1}$ nanoparticles. The OD630 of the solution was measured every few hours with a microplate reader (Elx808, BioTek, USA), and the bacterial growth curve was drawn accordingly.

The bacterial solution was Incubated at 37 °C for 14 h for *E. coli*, 6 h for *E. faecalis* and 24 h for *P. gingivalis*, diluted to $10^6$ and inoculated into agar plates. After incubation at 37 °C for 24 h, the developed colonies were counted.

### 4.14. Transcriptome sequencing of *E. coli*

A solution of *E. coli* ($10^6$ CFU $mL^{-1}$) was cultured with or without 10 μmol $L^{-1}$ NanoCr for 14 h. The *E. coli* culture was collected and submitted to Azenta Life Sciences (Nanjing, China), where transcriptome sequencing was performed.

### 4.15. SEM imaging of bacteria

A solution containing the bacteria at a concentration of $10^6$ CFU $mL^{-1}$ *E. coli*, $10^5$ CFU $mL^{-1}$ *E. faecalis* or $10^5$ CFU $mL^{-1}$ *P. gingivalis* was mixed with 10 μmol $L^{-1}$ NanoCr. The bacterial solution was incubated at 37 °C for 14 h for *E. coli*, 6 h for *E. faecalis*, and 24 h for *P. gingivalis*. The bacteria were washed with PBS and then fixed in 2.5% glutaraldehyde. The sample was dehydrated and observed by an SEM (JSM-7900F) coupled with an energy dispersive X-ray spectrometer. During the observation stage, X-ray signals were collected from 0 to 20 keV, 20 eV per channel. Elemental mapping was performed to obtain the spatial distribution of elements over the bacteria.

### 4.16. Determination of ATP levels

Quantification of the ATP levels in cultured bacterial cells was performed with a microbial cell viability assay (BacTiter-Glo, Promega, USA) according to the manufacturer's protocol. In brief, microbial cells in the culture medium were added to 96-well plates with 100 μL per well. Then, 100 μL of BacTiter-Glo Reagent was added to each well. The contents were briefly mixed and incubated for 5 min, and luminescence was measured with a microplate reader (FlexStation 3).

### 4.17. Statistical analyses

Data are presented as the means ± standard deviations. Student's *t* test was used to analyze the significance of differences between two groups. For comparisons among more than two groups, one-way ANOVA was used if the data passed the normality tests and was followed by Tukey's multiple comparison test for all pairs of groups. GraphPad PRISM version 9.0 was used for data management and statistical analyses. Values of $p < 0.05$*, $p < 0.01$**, $p < 0.001$*** and $p < 0.0001$**** were considered significant.

## Author contributions

Chuanda Zhu and Fei Xie as the co-authors contribute equally: conceptualization, performed the experiments, writing – original draft, read and approved the final manuscript. Lidong Gong and NingXin Zhu: provided assistance in designing and performing the experiments. Qiang Ma and Yuanyuan Yang: provided assistance in information searching. Xinrong Zhao: provided assistance in electron microscope photography; Man Qin: assisted in experiments designing. Zhiqiang Lin and Yuanyuan Wang: conceptualization, funding acquisition, writing – review & editing, read and approved the final manuscript.

## Conflicts of interest

There are no conflicts to declare.

## Acknowledgements

This work was supported by grants including Beijing Nature Science Foundation (Grant 7222222 to Y. W.), Peking University Medicine Fund of Fostering Young Scholar's Scientific & Technological Innovation A (grant BMU2022PY021 to Y. W.), Beijing Natural Science Foundation (grant L202049 and JQ21038 to Z. L.), the National Natural Science Foundation of China (grant U20A20412 to Q. Z.), China University Innovation Fund of Industry, Education and Research from Ministry of Education Science and Technology Development Center (grant 2021JH051 to Z. L., Special Project on the Wound Repair of Jianhe Healthcare), and the Fundamental Research Funds for the Central Universities (the Peking University Medicine Fund of Fostering Young Scholars' Scientific & Technological Innovation, grant BMU2022PY009 to Z. L.; the Peking University Medicine Special Fund for Talents, grant BMU2022RCZX016 to Z. L.).

## References

1 J. Baginska, E. Rodakowska, R. Milewski and A. Kierklo, *BMC Oral Health*, 2014, **14**, 74.
2 G. Aarabi, G. Heydecke and U. Seedorf, *Int. J. Mol. Sci.*, 2018, **19**, 1978.
3 S. Shabahang, *J. Endod.*, 2013, **39**, S26–S29.
4 M. Zanini, M. Hennequin and P.-Y. Cousson, *J. Endod.*, 2016, **42**, 1167–1174.
5 B. L. Colombini-Ishikiriama, T. J. Dionisio, T. F. Garbieri, R. A. da Silva, M. A. A. M. Machado, S. H. P. de Oliveira, V. S. Lara, A. S. Greene and C. F. Santos, *BMC Immunol.*, 2020, **21**, 38.
6 S. H. Zaky, M. Shehabeldin, H. Ray and C. Sfeir, *Eur. Cells Mater.*, 2021, **41**, 184–193.
7 Guideline on Pulp Therapy for Primary and Immature Permanent Teeth, *Pediatr. Dent.*, 2016, **38**, 280.
8 P. De Coster, S. Rajasekharan and L. Martens, *Int. J. Clin. Pediatr. Dent.*, 2013, **23**, 389–399.
9 N. Cohenca, A. Paranjpe and J. Berg, *Dent. Clin. North Am.*, 2013, **57**, 59–73.
10 P. Chailertvanitkul, J. Paphangkorakit, N. Sooksantisakoonchai, N. Pumas, W. Pairojamornyoot, N. Leela-apiradee and P. V. Abbott, *Int. Endod. J.*, 2014, **47**, 835–842.
11 P. Aguilar and P. Linsuwanont, *J. Endod.*, 2011, **37**, 581–587.

 

12 A. Parthasarathy, S. Kamat, M. Kamat and K. Kidiyoor, *J. Conserv. Dent.*, 2016, **19**, 274–279.
13 A. Qureshi, E. Soujanya, N. Kumar, P. Kumar and S. Hivarao, *J. Clin. Diagn. Res.*, 2014, **8**, 316–321.
14 C. Boutsiouki, R. Frankenberger and N. Krämer, *Eur. Arch. Paediatr. Dent.*, 2018, **19**, 297–309.
15 H. F. Duncan, K. M. Galler, P. L. Tomson, S. Simon, I. El-Karim, R. Kundzina, G. Krastl, T. Dammaschke, H. Fransson, M. Markvart, M. Zehnder and L. Bjørndal, *Int. Endod. J.*, 2019, **52**, 923–934.
16 C. Brizuela, A. Ormeño, C. Cabrera, R. Cabezas, C. I. Silva, V. Ramírez and M. Mercade, *J. Endod.*, 2017, **43**, 1776–1780.
17 T. Komabayashi, Q. Zhu, R. Eberhart and Y. Imai, *Dent. Mater. J.*, 2016, **35**, 1–12.
18 C. Manaspon, C. Jongwannasiri, S. Chumprasert, N. Sa-Ard-Iam, R. Mahanonda, P. Pavasant, T. Porntaveetus and T. Osathanon, *BMC Oral Health*, 2021, **21**, 209–213.
19 T. Giraud, C. Jeanneau, C. Rombouts, H. Bakhtiar, P. Laurent and I. About, *Dent. Mater.*, 2019, **35**, 24–35.
20 M. Parirokh and M. Torabinejad, *J. Endod.*, 2010, **36**, 16–27.
21 M. Torabinejad, C. U. Hong, T. R. P. Ford and J. D. Kettering, *J. Endod.*, 1995, **21**, 403–406.
22 G. Huang, J. Zang, L. He, H. Zhu, J. Huang, Z. Yuan, T. Chen and A. Xu, *ACS Nano*, 2022, **16**, 431–452.
23 J. Zhou, M. Li, Q. Chen, X. Li, L. Chen, Z. Dong, W. Zhu, Y. Yang, Z. Liu and Q. Chen, *Nat. Commun.*, 2022, **13**, 3432–3432.
24 N. Nantapong, R. Murata, S. Trakulnaleamsai, N. Kataoka, T. Yakushi and K. Matsushita, *Appl. Microbiol. Biotechnol.*, 2019, **103**, 5355–5366.
25 F. Cheng, S. Wang, H. Zheng, H. Shen, L. Zhou, Z. Yang, Q. Li, Q. Zhang and H. Zhang, *Small Methods*, 2022, **6**, 2200949–2200949.
26 H. Zhao, J. Huang, Y. Li, X. Lv, H. Zhou, H. Wang, Y. Xu, C. Wang, J. Wang and Z. Liu, *Biomaterials*, 2020, **258**, 120286–120286.
27 C. Tu, H. Lu, T. Zhou, W. Zhang, L. Deng, W. Cao, Z. Yang, Z. Wang, X. Wu, J. Ding, F. Xu and C. Gao, *Biomaterials*, 2022, **286**, 121597–121597.
28 Z. Yu, R. Lou, W. Pan, N. Li and B. Tang, *Chem. Commun.*, 2020, **56**, 15513–15524.
29 K. Yan, C. Mu, C. Zhang, Q. Xu, Z. Xu, D. Wang, X. Jing and L. Meng, *J. Colloid Interface Sci.*, 2022, **616**, 759–768.
30 S. Wang, H. Zheng, L. Zhou, F. Cheng, Z. Liu, H. Zhang, L. Wang and Q. Zhang, *Nano Lett.*, 2020, **20**, 5149–5158.
31 X. Bao, J. Zhao, J. Sun, M. Hu and X. Yang, *ACS Nano*, 2018, **12**, 8882–8892.
32 C. Zhu, Q. Ma, L. Gong, S. Di, J. Gong, Y. Wang, S. Xiao, L. Zhang, Q. Zhang, J. J. Fu, D. Lu and Z. Lin, *Acta Biomater.*, 2022, **141**, 429–439.
33 W. S. Zhang, E. H. Brück, Z. D. Zhang, O. Tegus, W. F. Li, P. Si, D. Y. Geng and K. H. J. Buschow, *Phys. B*, 2005, **358**, 332–338.
34 Z. Pei, X. Zheng and Z. Li, *J. Nanosci. Nanotechnol.*, 2016, **16**, 4655–4671.
35 Y. Sun, Y. Yin, L. Gong, Z. Liang, C. Zhu, C. Ren, N. Zheng, Q. Zhang, H. Liu, W. Liu, F. You, D. Lu and Z. Lin, *Nano Res.*, 2020, 1–13, DOI: 10.1007/s12274-020-3243-5.
36 V. Hirsch, M. Wolgin, A. V. Mitronin and A. M. Kielbassa, *Arch. Oral Biol.*, 2017, **82**, 38–46.
37 K. Nara, N. Kawashima, S. Noda, M. Fujii, K. Hashimoto, K. Tazawa and T. Okiji, *J. Cell. Physiol.*, 2019, **234**, 21331–21341.
38 Y. He, Y. Gan, J. Lu, Q. Feng, H. Wang, H. Guan and Q. Jiang, *J. Endod.*, 2016, **43**, 90–95.
39 T. Izumi, I. Kobayashi, K. Okamura and H. Sakai, *Arch. Oral Biol.*, 1995, **40**, 609–614.
40 J. Siqueira, I. Rôças, J. Provenzano, F. Daibert, M. Silva and K. Lima, *J. Endod.*, 2009, **35**, 1186–1192.
41 I. Prada, P. Micó-Muñoz, T. Giner-Lluesma, P. Micó-Martínez, N. Collado-Castellano and A. Manzano-Saiz, *Med. Oral. Patol. Oral. Cir. Bucal.*, 2019, **24**, e364–e372.
42 M. Barbosa-Ribeiro, R. Arruda-Vasconcelos, L. M. Louzada, D. G. dos Santos, F. D. Andreote and B. P. F. A. Gomes, *Clin. Oral. Investig.*, 2020, **25**, 2017–2027.
43 R. Zhu, C. Yang, K. Li, R. Yu, G. Liu and B. Peng, *J. Cleaner Prod.*, 2020, **277**, 123278.
44 A. C. Krauss, X. Gao, L. Li, M. L. Manning, P. Patel, W. Fu, K. G. Janoria, G. Gieser, D. A. Bateman, D. Przepiorka, Y. L. Shen, S. S. Shord, C. M. Sheth, A. Banerjee, J. Liu, K. B. Goldberg, A. T. Farrell, G. M. Blumenthal and R. Pazdur, *Clin. Cancer Res.*, 2019, **25**, 2685–2690.
45 M. Rai, A. P. Ingle, S. Birla, A. Yadav and C. A. D. Santos, *Crit. Rev. Microbiol.*, 2015, **42**, 1–24.
46 I. Gupta, N. Duran and M. Rai, *Nano-Antimicrobials*. Springer, Berlin, Heidelberg. 2012. pp. 525–548.
47 S.K. Shinde, N.D. Grampurohit, D.D. Gaikwad, S.L. Jadhav, M.V. Gadhave and P.K. Shelke, *Asian Pac. J. Trop. Dis.*, 2012, **2**, 331–334.
48 M. Horie, K. Nishio, S. Endoh, H. Kato, K. Fujita, A. Miyauchi, A. Nakamura, S. Kinugasa, K. Yamamoto, E. Niki, Y. Yoshida and H. Iwahashi, *Environ. Toxicol.*, 2013, **13**(28), 61–75.
49 T. Lawrence, *Cold Spring Harbor Perspect. Biol.*, 2009, **1**, a001651.
50 B. Kaminska, *Biochim. Biophys. Acta*, 2005, **1754**, 253–262.
51 M. Mittal, M. R. Siddiqui, K. Tran, S. P. Reddy and A. B. Malik, *Antioxid. Redox Signaling*, 2014, **20**, 1126–1167.
52 N. Bryan, H. Ahswin, N. Smart, Y. Bayon, S. Wohlert and J. A. Hunt, *Eur. Cells Mater.*, 2012, **24**, 249–265.
53 E. Naik and V. M. Dixit, *J. Exp. Med.*, 2011, **208**, 417–420.
54 A. Cuadrado and A. R. Nebreda, *Biochem. J.*, 2010, **429**, 403–417.
55 Y. V. Morimoto and T. Minamino, *Subcell. Biochem.*, 2021, **96**, 297–321.
56 S. Nakamura and T. Minamino, *Biomolecules*, 2019, **9**, 279.
57 T. C. Cullender, B. Chassaing, A. Janzon, K. Kumar, C. E. Muller, J. J. Werner, L. T. Angenent, M. E. Bell,

A. G. Hay, D. A. Peterson, J. Walter, M. Vijay-Kumar, A. T. Gewirtz and R. E. Ley, *Cell Host Microbe*, 2013, **14**, 571–581.
58 L. Laganenka, M. E. López, R. Colin and V. Sourjik, *mBio*, 2020, **11**, e02269–19.
59 B. Chaban, H. V. Hughes and M. Beeby, *Semin. Cell Dev. Biol.*, 2015, **46**, 91–103.
60 Z. Zhang, B. Li, Q. Cai, S. Qiao, D. Wang, H. Wang, H. Zhang, Y. Yang and W. Meng, *Biofouling*, 2021, **37**, 222–234.
61 S. Fulaz, S. Vitale, L. Quinn and E. Casey, *Trends Microbiol.*, 2019, **27**, 915–926.
62 J. R. Morones, J. L. Elechiguerra, A. Camacho, K. Holt, J. B. Kouri, J. T. Ramírez and M. J. Yacaman, *Nanotechnology*, 2005, **16**, 2346–2353.